Porphyrin-Based Organogels: Control of the Aggregation Mode by a Pyridine−Carboxylic Acid Interaction

ARTICLE *in* LANGMUIR · APRIL 2005

Impact Factor: 4.46 · DOI: 10.1021/la047070u · Source: PubMed

5 AUTHORS, INCLUDING:

Kenji Kaneko
Kyushu University
233 PUBLICATIONS **4,225** CITATIONS

SEE PROFILE

Masayuki Takeuchi
National Institute for Materials Science
192 PUBLICATIONS **5,432** CITATIONS

SEE PROFILE

Porphyrin-Based Organogels: Control of the Aggregation Mode by a Pyridine−Carboxylic Acid Interaction

Satoshi Tanaka,† Michihiro Shirakawa,† Kenji Kaneko,‡
Masayuki Takeuchi,*,† and Seiji Shinkai*,†

Department of Chemistry and Biochemistry, Graduate School of Engineering, Kyushu University, 6-10-1 Hakozaki, Higashi-ku, Fukuoka 812-8581, Japan, and HVEM Laboratory, Kyushu University, Fukuoka 812-8581, Japan

Received November 30, 2004. In Final Form: December 9, 2004

To find a new strategy for designing porphyrin-based organogelators, hydrogen-bond-donating (carboxylic acid)/accepting (pyridine) substituents or electron-donating (dialkylamino)/withdrawing (pyridine) substituents were introduced into peripheral positions of a porphyrin (**1cp** or **1ep**, respectively), and the gelation properties were compared with those of symmetrical reference compounds bearing two pyridyl substituents or two ester groups (**1pp** or **1ee**, respectively). It was found that the symmetrical molecules show a solubility that is quite inferior to that of **1cp** and **1ep** having a dipole moment and precipitate from most organic solvents. **1cp**, **1ep**, and **1ee** formed gels with cyclohexane, methylcyclohexane, and several alcoholic solvents, but scanning electron microscopy (SEM) and transmission electron microscopy (TEM) observations revealed that their superstructures constructed in the organogels are very different. In cyclohexane, **1cp** resulted in a sheetlike structure, whereas **1ep** and **1ee** resulted in a fiberlike structure. The difference is attributed to the two-dimensional interactive forces in **1cp** consisting of the porphyrin−porphyrin $\pi-\pi$ stacking and the carboxylic acid−pyridine hydrogen bonding. In fact, when the hydrogen-bonding interaction was weakened by alcoholic solvents or by adding pyridine or *N*,*N*-(dimethylamino)-pyridine, the sheetlike structure was transfigured to the fiberlike structure. Further detailed analyses of their aggregation modes were conducted by spectroscopic methods such as ultraviolet−visible (UV−vis) absorption, Fourier transform infrared (FT-IR), and X-ray diffraction (XRD). On the basis of these findings, the influence of these peripheral substituents on the gel formation and the aggregation mode was discussed.

Introduction

One-dimensional alignment of porphyrins and phthalocyanines is of much concern in relation to the creation of novel supramolecular architectures such as nanowires, discotic liquid crystals, and helical ribbon structures.[1−5] This molecular assembling approach is also of significance in relation to the functional facets such as catalysts and light-harvesting systems.[6] The major driving force of these structures is considered to be a $\pi-\pi$ stacking interaction inherent to their π-conjugated skeletons. More recently, other supramolecular architectures constructed in organogels have attracted the widespread attention of supramolecular chemists, and the origin of organogel formation is considered to be a one-dimensional alignment of gelator molecules supported by van der Waals interactions and/or hydrogen-bonding interactions.[7,8] This concept presents a new field for porphyrin and phthalocyanine chemistry, in that they could act as powerful building blocks for the design of a new gelator, whereas, before, these compounds tended to just assemble into a one-dimensional supramolecular architecture.[9] In addition, we found that many new hydrogen-bond-based gelators can be developed by using a natural library of carbohydrate

* To whom correspondence should be addressed. E-mail: taketcm@mbox.nc.kyushu-u.ac.jp (M.T.); seijitcm@mbox.nc.kyushu-u.ac.jp (S.S.).

† Graduate School of Engineering.

‡ HVEM Laboratory.

(1) (a) Nostrum, C. F.; Picken, S. J.; Schouten, A.-J.; Nolte, R. J. M. *J. Am. Chem. Soc.* **1995**, *117*, 9957−9965. (b) Schenning, A. P. H.; Benneker, F. B. G.; Geurts, H. P. M.; Liu, X. Y.; Nolte, R. J. M. *J. Am. Chem. Soc.* **1996**, *118*, 8549−8552. (c) Nostrum, C. F.; Nolte, R. J. M. *Chem. Commun.* **1996**, 2385−2392. (d) Engelkamp, H.; Nostrum, C. F.; Picken, S. J.; Nolte, R. J. M. *Chem. Commun.* **1998**, 979−980. (e) Engelkamp, H.; Middelbeek, S.; Nolte, R. J. M. *Science* **1999**, *284*, 785−788. (f) Samori, S.; Engelkamp, H.; Witte, P.; Rowan, A. E.; Nolte, R. J. M.; Rabe, J. P. *Angew. Chem.* **2001**, *113*, 2410−2412. (g) Lensen, M. C.; van Dingenen, S. J. T.; Elemans, J. A. A. W.; Dijkstra, H. P.; van Klink, G. P. M.; van Koten, G.; Gerritsen, J. W.; Speller, S.; Nolte, R. J. M.; Rowan, A. E. *Chem. Commun*. **2004**, 762−763. (h) Lensen, M. C.; Takazawa, K.; Elemans, J. A. A. W.; Jeukens, C. R. L. P. N.; Christianen, P. C. M.; Maan, J. C.; Rowan, A. E.; Nolte, R. J. M. *Chem.—Eur. J*. **2004**, *10*, 831−839.

(2) (a) Fuhrhop, J.-H.; Demoulin, C.; Boettcher, C.; Koning, J.; Siffel, U. *J. Am. Chem. Soc.* **1992**, *114*, 4159−4165. (b) Fuhrhop, J.-H.; Bindig, U.; Siggel, U. *J. Am. Chem. Soc.* **1993**, *115*, 11036−11037. (c) Bindig, U.; Schulz, A.; Fuhrhop, J.-H. *New J. Chem.* **1995**, *19*, 427−435 and references therein.

(3) (a) Smolenyak, P.; Peterson, R.; Nebesny, K.; Torker, M.; O'Brien, D. F.; Armstrong, N. R. *J. Am. Chem. Soc.* **1999**, *121*, 8628−8636. (b) Drager, S. A.; Zangmeister, R. A. P.; Armstrong, N. R.; O'Brien, D. F. *J. Am. Chem. Soc.* **2001**, *123*, 3595−3596.

(4) (a) Kimura, M.; Kitamura, T.; Muto, T.; Hanabusa, K.; Shirai, H.; Kobayashi, N. *Chem. Lett.* **2000**, 1088−1089. (b) Kimura, M.; Muto, T.; Takimoto, H.; Wada, K.; Ohta, K.; Hanabusa, K.; Shirai, H.; Kobayashi, N. *Langmuir* **2000**, *16*, 2078−2082. (c) Kimura, M.; Wada, K.; Ohta, K.; Hanabusa, K.; Shirai, H.; Kobayashi, N. *J. Am. Chem. Soc.* **2001**, *123*, 2438−2439.

(5) (a) Imada, T.; Murakami, H.; Shinkai, S. *Chem. Commun.* **1994**, 1557−1558. (b) Arimori, S.; Takeuchi, M.; Shinkai, S. *J. Am. Chem. Soc.* **1996**, *118*, 245−246. (c) Arimori, S.; Takeuchi, M.; Shinkai, S. *Supramol. Sci.* **1998**, *5*, 1−8.

(6) Kadish, K. M.; Smith, K. M.; Guilard, R. *The Porphyrin Handbook*; Academic Press: San Diego, CA, 1900; Vol. 6, pp 1−131.

(7) Luboradzki, R.; Gronwald, O.; Ikeda, M.; Shinkai, S.; Reinhoudt, D. N. *Tetrahedron* **2000**, *56*, 9595−9599.

(8) For comprehensive reviews for organogels, see: (a) Esch, J.; Schoonbeek, F.; Loos, M.; Kooijman, H.; Veen, E. M.; Kellogg, R. M.; Feringa, B. L. In *Supramolecular Science: Where It Is and Where It Is Going*; Ungaro, R., Dalcanale, E., Eds.; Kluwer: Dordrecht, The Netherlands, 1999; pp 233−259. (b) Melendez, R. E.; Carr, A. J.; Linton, B. R.; Hamilton, A. D. *Struct. Bonding* **2000**, 31−61. (c) Shinkai, S.; Murata, K. *J. Mater. Chem.* **1998**, *8*, 485−495.

(9) We found that certain cholesterol-appended porphyrins act as gelators of organic solvent: (a) Ishi-i, T.; Jung, J. H.; Shinkai, S. *J. Mater. Chem.* **2000**, *10*, 2238−2240. (b) Tian, H. J.; Inoue, K.; Yoza, K.; Ishi-i, T.; Shinkai, S. *Chem. Lett.* **1998**, 871−872. In these organogels, however, it is considered that porphyrin moieties are located around a helical central column of cholesterol moieties, like a spiral staircase.

10.1021/la047070u CCC: $30.25
Published on Web 02/09/2005

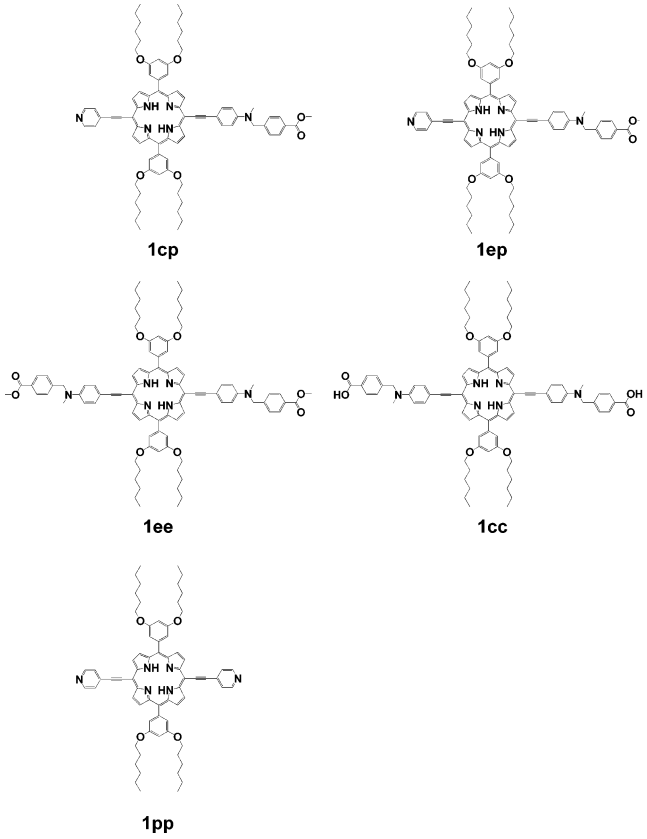

molecules as hydrogen-bonding sites.[10−12] Recently, we found that one-dimensional aggregates composed of porphyrins are "reinforced" or "modulated" by the peripheral hydrogen-bonding interaction among covalently appended saccharides and/or amide groups to the central porphyrin column.[13] It thus occurred to us that porphyrin molecules, the periphery of which is modified with hydrogen-bond-donating/accepting groups or electron-donating/withdrawing groups perpendicular to the porphyrin−porphyrin $\pi-\pi$ stacking axis,[14] would show novel one- or two-dimensional aggregation properties as a result of the synergistic effect of porphyrin−porphyrin $\pi-\pi$ stacking and "orthogonal" hydrogen-bonding or dipole−dipole interactions. With this idea in mind, we synthesized porphyrins **1cp**, **1ep**, **1ee**, **1pp**, and **1cc** and evaluated the influence of these peripheral substituents on the gelation and the morphology.

Table 1. Gelation Properties of 1cp, 1ep, and 1ee[a]

solvent	1cp	1ep	1ee
benzene	F	S	S
cyclohexane	G	G	G
methylcyclohexane	G	G	G
t-butanol	G	Fp	Fp
2-propanol	G	Fp	Fp
methanol	G	Fp	Fp

[a] [gelator], 1.00 wt %; G, gel; F, viscous fluid; Fp, turbid fluid with some precipitate; S, soluble.

Results and Discussion

Gelation Test. The gelation properties of five porphyrin derivatives have been tested for several selected protic/aprotic and polar/apolar solvents. The gelator was mixed in a capped test tube with the appropriate amount of solvent, and the mixture was heated until the solid was dissolved. The sample was cooled in air to 25 °C, left for 1 h at this temperature, and then turned upside down. When the fluidity of the solvent was suppressed, it was denoted by a "G" in Table 1. In some cases, the gels were opaque or slightly turbid, indicating that this series of porphyrin-based gelators tends to form microcrystals ("Fp" in Table 1).

It is seen from Table 1 that **1cp** is capable of gelating several organic solvents such as cyclohexane, methylcyclohexane, and alcoholic solvents. One can presume that both the porphyrin−porphyrin $\pi-\pi$ stacking and the carboxylic acid−pyridine hydrogen-bonding interaction are operative in aprotic solvents, whereas only the $\pi-\pi$ stacking is mainly operative in protic solvents as a driving force for molecular association. The gelation properties for **1cp** show that the gels are formed in both aprotic and protic solvent systems, but the difference in the dimension of its molecular aggregation pattern of **1cp** should be reflected by the superstructures constructed in each solvent (*vide post*).

To understand the role of the carboxylic acid group more clearly, we synthesized **1ep**, **1ee**, **1cc**, and **1pp**. Compound **1cc** formed the precipitate in most organic solvents because of its poor solubility arising from the two carboxylic acid groups. Although **1pp** was soluble in benzene, it resulted in the precipitate from cyclohexane, methylcyclohexane, and alcoholic solvents. Since **1ep** and **1ee** are also soluble in benzene (Table 1), one may presume that benzene weakens the $\pi-\pi$ stacking interaction among the gelators and solvates these molecules. These results suggest that, in **1cp** bearing one acid group and one base group, the crystal growth leading to the precipitation is suppressed by the acid−base interaction, which rather facilitates the growth of alternative aggregate structures suitable for gel formation in the solvent system tested herein. On the other hand, **1ep** and **1ee** gelated cyclohexane and methylcyclohexane, but the precipitates were formed from alcoholic solvents. These results imply that, in the gel formation of **1cp** in alcoholic solvents, the carboxylic acid group is "masked" by solvent alcohol molecules. One can regard, therefore, that the porphyrin−porphyrin $\pi-\pi$ stacking plays a central role in arranging these molecules in a one-dimensional direction.

The relative stability of the gels prepared from **1cp**, **1ep**, and **1ee** was compared with the concentration dependence and the gel-to-sol phase transition temperature (T_{gel}). As summarized in Table 2, the gelator, which immobilizes cyclohexane at the lowest concentration, is

(10) (a) Yoza, K.; Ono, Y.; Yoshihara, K.; Akao, T.; Shinmori, H.; Takeuchi, M.; Shinkai, S.; Reinhoudt, D. N. *Chem. Commun.* **1998**, 907−908. (b) Yoza, K.; Amanokura, N.; Ono, Y.; Akao, T.; Shinmori, H.; Shinkai, S.; Reinhoudt, D. N. *Chem.—Eur. J.* **1999**, *5*, 2722−2729. (c) Amanokura, N.; Akao, T.; Shinmori, H.; Shinkai, S.; Reinhoudt, D. N. *J. Chem. Soc., Perkin Trans. 2* **1998**, 2585−2591. (d) Gronwald, O.; Sakurai, K.; Luboradzki, R.; Kimura, T.; Shinkai, S. *Carbohydr. Res.* **2001**, *331*, 307−318.

(11) For a comprehensive review for sugar-based gelators, see: Gronwald, O.; Shinkai, S. *Chem.—Eur. J.* **2001**, *7*, 4328−4334.

(12) Luboradzki, R.; Gronwald, O.; Ikeda, A.; Shinkai, S. *Chem. Lett.* **2000**, 1148−1149.

(13) (a) Tamaru, S.-i.; Nakamura, M.; Takeuchi, M.; Shinkai, S. *Org. Lett.* **2001**, *3*, 3631−3634. (b) Tamaru, S.-i.; Uchino, S.; Takeuchi, M.; Ikeda, M.; Hatano, T.; Shinkai, S. *Tetrahedron Lett.* **2002**, *43*, 3751−3755. (c) Shirakawa, M.; Kawano, S.-i.; Fujita, N.; Sada, K.; Shinkai, S. *J. Org. Chem.* **2003**, *68*, 5037−5044. (d) Shirakawa, M.; Fujita, N.; Shinkai, S. *J. Am. Chem. Soc.* **2003**, *125*, 9902−9903. (e) Kawano, S.-i.; Tamaru, S.-i.; Fujita, N.; Shinkai, S. *Chem.—Eur. J.* **2004**, *10*, 343−351.

(14) (a) Bhyrappa, P.; Wilson, S. R.; Suslick, K. S. *J. Am. Chem. Soc.* **1997**, *119*, 8492−8502. (b) Bhyrappa, P.; Wilson, S. R.; Suslick, K. S. *Supramol. Chem.* **1998**, *9*, 169−174. (c) Tanaka, T.; Endo, K.; Aoyama, Y. *Bull. Chem. Soc. Jpn.* **2001**, *74*, 907−916. (d) Terech, P.; Scherer, C.; Deme, B.; Ramasseul, R. *Langmuir* **2003**, *19*, 10641−10647. (e) Yamaguchi, T.; Ishii, N.; Tashiro, K.; Aida, T. *J. Am. Chem. Soc.* **2003**, *125*, 13934−13935. (f) Yamaguchi, T.; Kimura, T.; Matsuda, H.; Aida, T. *Angew. Chem., Int. Ed.* **2004**, *43*, 6350−6355.

Table 2. Concentration Dependence and T_{gel} for 1cp, 1ep, and 1ee in Cyclohexane[a]

	concentration			
gelator	1.00 wt % (T_{gel})	0.75 wt %	0.50 wt %	0.25 wt %
1cp	G (46 °C)	G	F	F
1ep	G (31 °C)	G	G	F
1ee	G (29 °C)	G	G	G

[a] For the notation, see footnote *a* of Table 1.

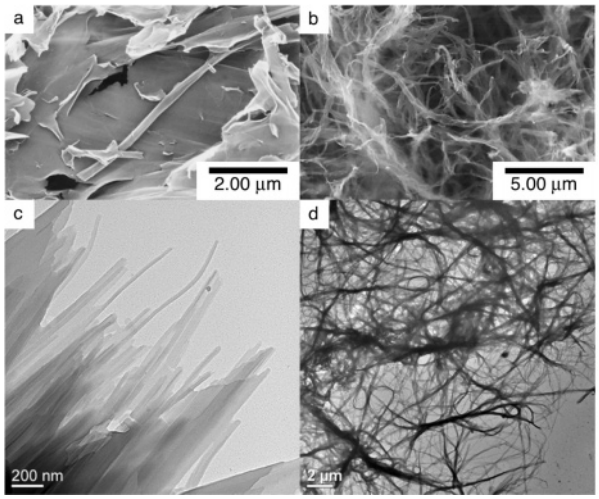

Figure 1. SEM images of xerogels prepared from (a) a **1cp** (1.00 wt %) + cyclehexane gel and (b) a **1cp** (1.00 wt %) + *t*-butanol gel and TEM images of (c) **1cp** (0.05 wt %) + cyclohexane and (d) **1cp** (0.05 wt %) + *t*-butanol.

1ee, and the next is **1ep**. As seen from their scanning electron microscopy (SEM) and transmission electron microscopy (TEM) images (*vide infra*), **1ee** tends to form a straight fiber, suggesting that the molecular association and the growth of the fibrous structure can occur most advantageously. This may lead to the gelation ability at the low-concentration region. On the other hand, **1cp** tends to form a sheetlike structure utilizing both of the porphyrin−porphyrin $\pi-\pi$ stacking and the carboxylic acid−pyridine hydrogen-bonding interaction (*vide post*). Thus, the association should proceed by adjusting the interactions between these two different intermolecular forces. Presumably, this is why the gelation cannot be observed up to [**1cp**] = 0.50 wt %. In contrast, the T_{gel} values appear in the order of **1cp** > **1ep** > **1ee**. We consider, therefore, that once the gel is formed with **1cp**, the molecular dissociation accompanies cleavage of these two intermolecular forces. Thus, its T_{gel} can be higher than those for **1ep** and **1ee**.

SEM and TEM Observations. To find a possible correlation between the intermolecular forces operating between gelators and the resultant aggregate structures, we characterized the morphology using SEM and TEM. In a gel of **1cp** + cyclohexane, the two-dimensional intermolecular forces, consisting of the $\pi-\pi$ stacking and the hydrogen bonding, should be operative. As seen in Figure 1a, this system results in a sheetlike, two-dimensional structure. At [**1cp**] = 0.05 wt %, the mixture still retains the fluidity. The importance and the versatility of a carboxylic acid−pyridine couple as a building block in molecular assemblies have been emphasized by Kato's group.[15] The present results also establish that the molecular assembly or **1cp** constructed in cyclohexane has a two-dimensional factor arising from the porphyrin−porphyrin $\pi-\pi$ stacking and the carboxylic acid−pyridine hydrogen-bonding interaction. The TEM image of this mixture (Figure 1c) establishes that the sheetlike structure

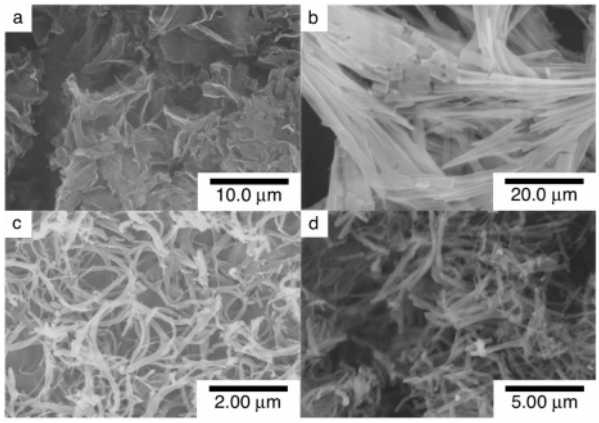

Figure 2. SEM images of xerogels prepared from a **1cp** (1.00 wt %) + cyclohexane gel in the presence of (a) 10 mol equiv of pyridine, (b) 100 mol equiv of pyridine, (c) 10 mol equiv of DMAP, and (d) 100 mol equiv of DMAP.

is already constructed at such a low concentration region. Figure 1b shows a SEM image of a gel formed from **1cp** + *t*-butanol. In contrast to a sheetlike structure in Figure 1a, it features a fiberlike, one-dimensional structure. One may thus consider that solvation of the carboxylic acid group by *t*-butanol molecules changes the aggregation mode into the one-dimensional pattern, and the fibrous structure appears as a typical assembly produced from the one-dimensional aggregation. Even in the sol phase at [**1cp**] = 0.05 wt %, one can still recognize the presence of such a fibrous structure (Figure 1d).

Here, it occurred to us that the addition of a small amount of pyridine might change the two-dimensional aggregation mode of **1cp** + cyclohexane gel to the one-dimensional one. Parts a and b of Figure 2 show SEM images of xerogels obtained from a **1cp** + cyclohexane gel in the presence of 10 and 100 mol equiv of pyridine, respectively. It is seen from these pictures that the sheetlike structure of **1cp** is cracked into subdivided pieces, and the fiberlike structure begins to grow. When *N*,*N*-(dimethylamino)pyridine (DMAP), the basicity of which is stronger than that of pyridine, is added, the sheetlike morphology is entirely converted to the fiberlike morphology (Figure 2c and d). These results indicate that added pyridine and DMAP can play a role to suppress the intermolecular carboxylic acid−pyridine interaction and to change the two-dimensional aggregation mode into the one-dimensional one; that is, the addition of a small amount of DMAP is sufficient to change the aggregation mode observed in cyclohexane to that observed in alcoholic solvents. Since the **1cp** + cyclohexane system still gives the gels even in the presence of 100 mol equiv of pyridine or DMAP, one can regard that the primary driving force stabilizing the gel network structure is the porphyrin−porphyrin $\pi-\pi$ stacking.

Compounds **1ep** and **1ee** both gelate cyclohexane and methylcyclohexane. Since **1ep** has a dipole across the porphyrin ring whereas **1ee** is a symmetrical molecule without such a dipole, we expected that this difference would be reflected by their aggregation morphology. Figure 3a and b shows the SEM images of xerogels prepared from a **1ep** + cyclohexane gel. Basically, it forms a network structure characteristic of an organogel system, and each

(15) (a) Kato, T.; Kubota, Y.; Nakano, M.; Uryu, T. *Chem. Lett.* **1995**, 1127−1128. (b) Kato, T.; Fukumasa, M.; Fréchet, J. M. J. *Chem. Mater.* **1995**, *7*, 368−372. (c) Kato, T.; Fukumasa, Y.; Uryu, T.; Ujiie, S. *Angew. Chem., Int. Ed. Engl.* **1997**, *36*, 1617−1618. (d) Kato, T.; Ihata, O.; Ujiie, S.; Tokita, M.; Watanabe J. *Macromolecules* **1998**, *31*, 3551−3555.

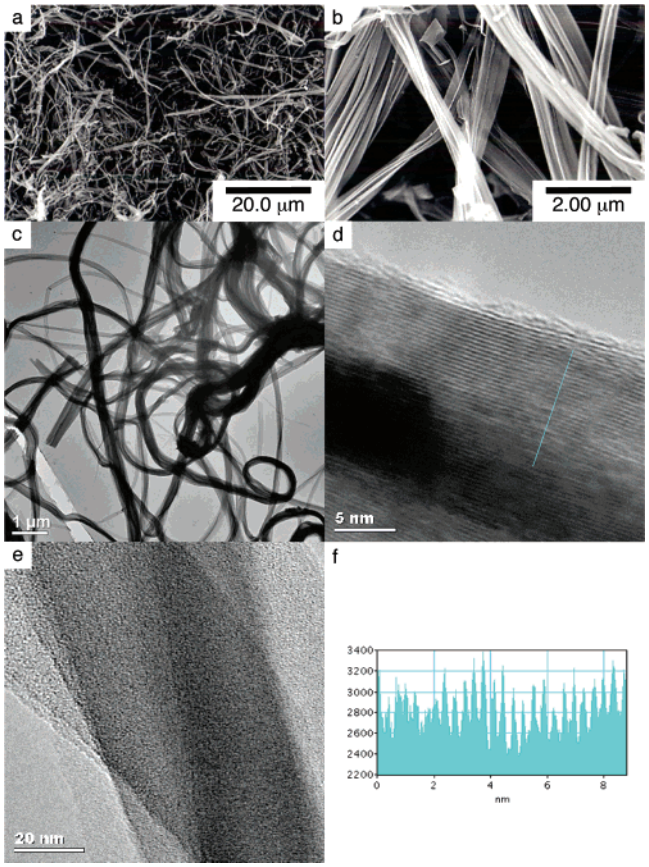

Figure 3. (a and b) SEM images of xerogels prepared from a **1ep** (1.00 wt %) + cyclohexane gel, (c) TEM image of **1ep** (0.05 wt %) + cyclohexane, (d and e) high-resolution TEM images of **1ep** (0.05 wt %) + cyclohexane, and (f) cross-sectional analysis of part d.

fiber consists of microfibrils; in total, the fiber looks like a stem of celery. In the fluid solution containing the low concentration of **1ep** (0.05 wt %), the aggregate shows a fibrous structure with a meandering conformation, and each fiber shows a light-and-shade contrast (Figure 3c). To obtain a further minute image of this structure, we observed one fiber with high-resolution TEM. As shown in Figure 3d, one fiber consists of many lamellae, the space distance of which is estimated to be 0.33 nm from its cross-sectional analysis (Figure 3f). This distance is comparable with that of two porphyrins which are associated by the $\pi-\pi$ stacking interaction.[16] One can also observe a platelike structure without a lamellar pattern (Figure 3e). We consider that this image is obtained when Figure 3d is observed from a perpendicular direction. The SEM and TEM images of a **1ee** + cyclohexane system are shown in Figure 4. Basically, the superstructure is similar to that of a **1ep** + cyclohexane system, but the fibers are more or less straight, compared with those obtained from a **1ep** + cyclohexane system. We consider that the high symmetry of the molecular structure in **1ee** is advantageous to grow as crystal-like straight fibers.

Spectroscopic Analyses. Spectroscopic discrimination between the H versus J porphyrin−porphyrin stacking is achieved by ultraviolet−visible (UV−vis) absorption spectral examinations. In the Soret band, the blue shift is a sign of the H-aggregate formation, whereas the red shift is a sign of the J-aggregate formation.[17] In the gel phase, the gelator concentrations were so high that the

(16) Hunter C. A.; Sanders, J. K. M. *J. Am. Chem. Soc.* **1990**, *112*, 5525−5534.

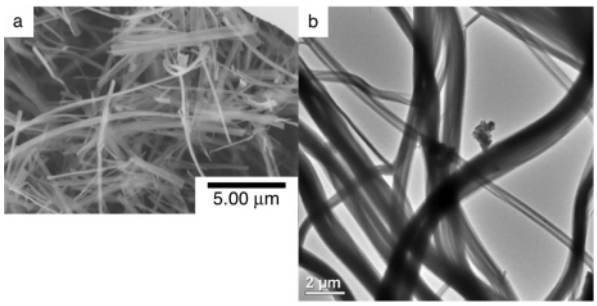

Figure 4. (a) SEM image of a xerogel prepared from a **1ee** (1.00 wt %) + cyclohexane gel and (b) TEM image of **1ee** (0.05 wt %) + cyclohexane.

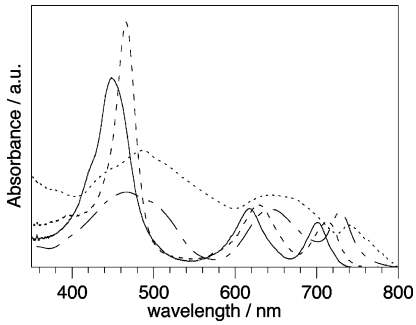

Figure 5. UV−vis absorption spectra of **1cp** (1.0×10^{-6} M) in CH_2Cl_2 (—), **1cp** (1.00 wt %) + cyclohexane gel (— - — - —), **1ee** (1.0×10^{-6} M) in CH_2Cl_2 (- - - -), and **1ee** (1.00 wt %) + cyclohexane gel (· · · · ·) at 25 °C. The spectra for **1cp** (1.00 wt %) + 2-propanol gel and **1ep** (1.00 wt %) + cyclohexane gel are not shown here for clarity (see text).

spectra could not be obtained using a conventional optical cell. Thus, the gel phase spectra were measured with a gel sample sandwiched by two quartz glass plates, so that the ordinate is expressed with an arbitrary unit.

As shown in Figure 5, the absorption maxima for a Soret band and two Q-bands appear at 448.3, 616.3, and 700.2 nm, respectively, in a homogeneous CH_2Cl_2 solution of **1cp**. In the gel systems of **1cp**, the peaks are significantly broadened, and both the Soret band and the Q-bands are shifted to longer wavelengths. The spectral shape for a **1cp** + 2-propanol gel[18] (not shown in Figure 5) is similar to that for a **1cp** + cyclohexane gel, but the red shifts in the spectral maxima for the **1cp** + 2-propanol gel are larger than those for the **1cp** + cyclohexane gel, that is, 22.4, 33.9, and 31.9 nm for the former and 17.3, 26.7, and 28.3 nm for the latter. The UV−vis absorption spectrum for a **1ep** + cyclohexane gel (not shown in Figure 5) is similar to those for the **1cp** gels, but the red shift of the Soret band is much larger (40.8 nm). One can propose, therefore, that the **1ep** + cyclohexane gel also adopts a J-aggregate, and this shift difference suggests that, in the J-aggregates, the porphyrin face-to-face stack of **1ep** slips out more largely than that of **1cp**.

The UV−vis absorption spectrum for a **1ee** + cyclohexane gel (Figure 5) is basically similar to those of the preceding gels, with a red shift of the Soret band by 18.8 nm. It should be noted, however, that in this spectrum there is a large shoulder at around 430 nm, which corresponds to a shift to a shorter wavelength by more than 30 nm. We now consider that the **1ee** + cyclohexane

(17) (a) Kano, K.; Fukada, K.; Wakami, H.; Nishiyabu, R.; Pasternack, R. F. *J. Am. Chem. Soc.* **2000**, *122*, 7494−7502. (b) Olada, S.; Segawa, H. *J. Am. Chem. Soc.* **2003**, *125*, 2792−2796.

(18) The use of *t*-butanol for the measurement of UV−vis absorption spectra was very difficult, because *t*-butanol readily solidified by itself, so that we here used 2-propanol instead of *t*-butanol.

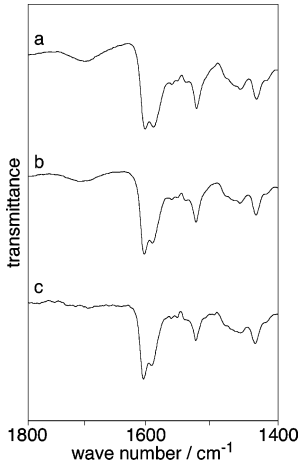

Figure 6. FT-IR spectra of (a) a solid powder of **1cp** and xerogels prepared from (b) a **1cp** (1.00 wt %) + cyclohexane gel and (c) a **1cp** (1.00 wt %) + *t*-butanol gel.

gel is constructed by a mixture of the J-aggregate and the H-aggregate or the J aggregate with a short slipping distance.[17b]

Fourier transform infrared (FT-IR) spectra of a **1cp** + cyclohexane gel, a **1cp** + *t*-butanol gel, and the solid powder are shown in Figure 6. It is known that when the pyridine nitrogen interacts with the carboxylic acid group, the $\nu_{C=N}$ band shifts from 1590 to 1600 cm^{-1}.[19] In the solid powder sample, these two bands appear at a similar intensity. In the gel samples, the intensity of the 1600 cm^{-1} band is stronger than that of the 1590 cm^{-1} band. The difference suggests that the carboxylic acid−pyridine interaction occurs more efficiently in the gel phase. Previously, we prepared several sugar-based gelators and assessed the formation of their hydrogen-bonding network by FT-IR.[10,19c]

It was shown that the gelators in the gel phase have both hydrogen-bonded and non-hydrogen-bonded OH groups, whereas those in the solid state have no non-hydrogen-bonded OH groups.[10,19c] This fact indicates that, in general, the intermolecular hydrogen bonding can occur more preferentially in the solid state because of the 3-D molecular packing. The contrasting results obtained from the **1cp** gels suggest, therefore, that the pyridine nitrogens and the carboxylic acid groups can favorably interact in the one-dimensional fibrous structure or in the two-dimensional sheet structure, presumably because of its structural characteristic that these two groups are arranged in a linear fashion sandwiching a porphyrin nucleus.

XRD Spectra: How Are Porphyrins Assembled in the Gel Phase? As shown in Figure 7, the xerogels prepared from the cyclohexane gels of **1cp**, **1ep**, and **1ee** gave X-ray diffraction (XRD) peaks at 2θ (d) = 5.7° (1.7 nm), 4.7° (2.1 nm), and 5.3° (1.9 nm), respectively. The XRD spectrum of the xerogel for **1ee** shows additional peaks at 6.1° (1.6 nm), 12.6° (0.78 nm), 19.6° (0.50 nm), 20.9° (0.47 nm), and 22.7° (0.43 nm), suggesting that, in accord with the UV−vis absorption spectrum (Figure 5), this xerogel is a mixture of the J-aggregate and the H-aggregate rather than the J-aggregate with a short slipping distance. Taking these XRD spectral data into account, we here discuss the influence of the peripheral substituents on the aggregation mode of these gelators (mainly, on **1cp** and **1ep**).

(19) (a) Kato, T.; Fréchet, J. M. J. *Macromolecules* **1989**, *22*, 3818−3819. (b) Lee, J. Y.; Painter, P. C.; Coleman, M. M. *Macromolecules* **1988**, *21*, 954−960. (c) Amaike, M.; Kobayashi, H.; Shinkai, S. *Bull. Chem. Soc. Jpn.* **2000**, *73*, 2553−2558.

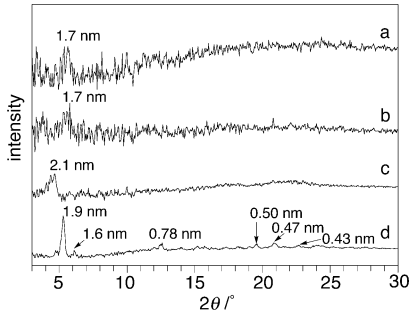

Figure 7. XRD patterns of xerogels prepared from organogels of (a) **1cp** (1.00 wt %) + cyclohexane, (b) **1cp** (1.00 wt %) + *t*-butanol, (c) **1ep** (1.00 wt %) + cyclohexane, and (d) **1ee** (1.00 wt %) + cyclohexane.

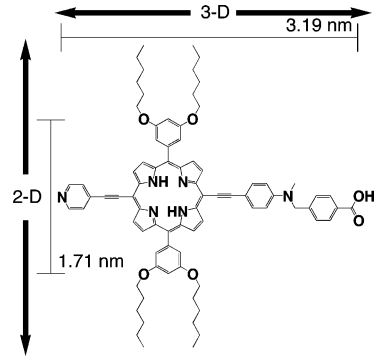

Figure 8. Molecular size of **1cp** estimated from computational energy minimization (Insight II, Discover-3). The length of the 2-D axis is common for **1ep** and **1ee**. The length of the 3-D axis is 3.37 nm for **1ep** and 4.53 nm for **1ee**.

First, an image obtained from high-resolution TEM (Figure 3d) clearly supports the view that the porphyrins are arranged in a distance of the conventional porphyrin−porphyrin $\pi-\pi$ stacking.[16] When this stacking direction is assigned to the 1-D axis, another image (Figure 3e) establishes that the porphyrins construct a platelike structure in the 2-D and 3-D axes.

In Figure 8, the molecular size of these gelators is illustrated; for example, **1cp** has a short axis (2-D) of 1.71 nm and a long axis (3-D) of 3.19−4.53 nm. The d values of 1.7−2.1 nm obtained from the XRD spectra well coincide with those of the 2-D short axis. One may propose, therefore, that the short axis consists of the porphyrin stacks without a porphyrin skeleton slip; that is, the next porphyrin exists right above the concerned porphyrin (Figure 9). As the short axis is constructed from two 3,5-di-*n*-hexyloxyphenyl groups and has no significant dipole because of its symmetrical structure, this no-slipping stacking mode is reasonably acceptable.

On the other hand, the long axis of the porphyrin should stack with a significant porphyrin skeleton slip (Figure 9), because the long axis is constructed from electron push−pull-type substituents and adopts, as shown by the UV−vis absorption spectrum (Figure 5), a J-aggregation mode. In the XRD spectrum, this long axis is expected to appear in a small angle region (2θ = 2.1−4.1°), which is difficult to identify by the present XRD apparatus.

Then, why does the SEM image of the **1cp** + cyclohexane gel afford a sheetlike structure (Figure 2), whereas that of the **1ep** + cyclohexane gel affords a fiberlike structure (Figure 3)? The long axis of both **1cp** and **1ep** has a dipole arising from the push−pull-type substituents. The basic difference is that only **1cp** has an additional intermolecular force arising from the hydrogen-bonding interaction. In the short axis direction of the 2-D/3-D plane,

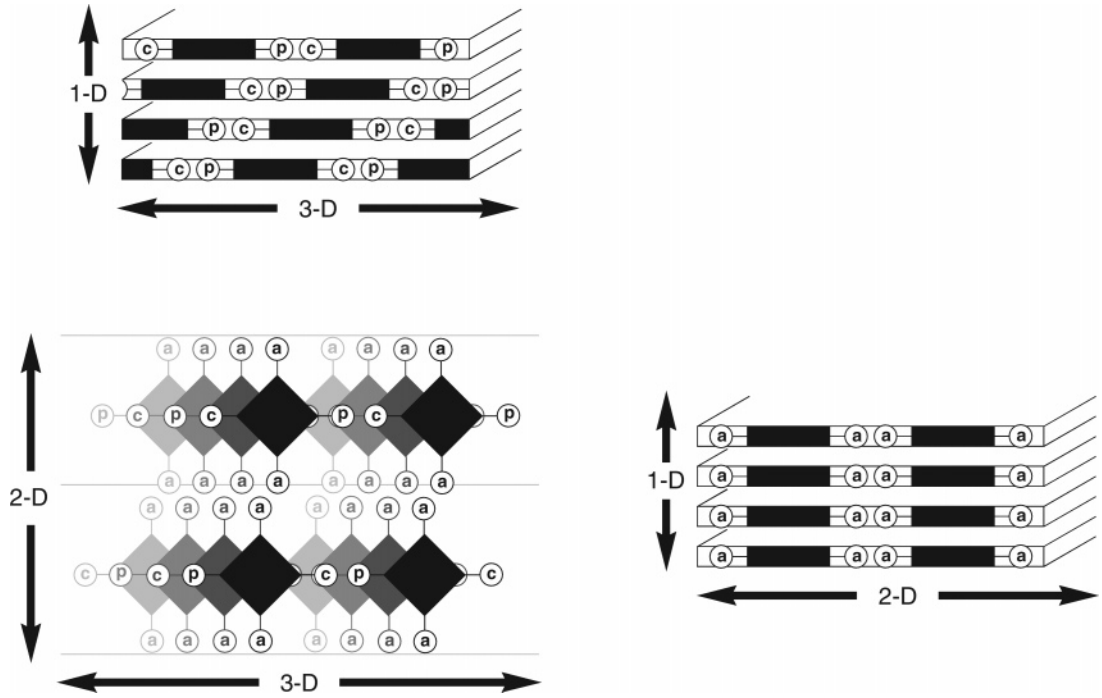

Figure 9. Aggregation modes of porphyrin-based gelators proposed on the basis of spectroscopic and microscopic analysis: a, di-*n*-hexyloxyphenyl group; c, carboxylic group; p, pyridyl group.

the 3,5-di-*n*-hexyloxyphenyl groups should be interdigitated with each other and in the 1-D direction the porphyrin skeletons are closely stacked. This aggregation mode would make it energetically difficult to bend the plate structure along the 2-D axis direction. In the long axis of **1cp**, the hydrogen-bonding interaction is operative between the carboxylic acid group and the pyridyl group, which would also make it difficult to bend the plate structure along this 3-D axis direction. As a result, one can observe a sheetlike structure for the SEM image of the xerogel prepared from a **1cp** + cyclohexane gel. In contrast, in the 3-D long axis of **1ep**, there is no such strong intermolecular interaction, which would make it possible to construct a curved surface. If the 2-D short axis direction is not bent while the 3-D long axis direction is curved, the resultant morphology can become a fiberlike structure.

As a summary of the foregoing findings and discussions, one may propose the aggregation mode shown in Figure 9 as the most likely assembling pattern.

Conclusion

Porphyrins *a priori* tend to assemble into the one-dimensional direction due to their $\pi-\pi$ stacking interaction, suggesting that their basic skeleton is suitable for the design of organogelators. The present study demonstrated that the one-dimensional aggregation mode can be further modulated by the combination of peripheral substituents such as electron-donating/withdrawing groups and hydrogen-bond-donating/accepting groups. We found that the systematic analyses of the spectral and microscopic data enable us to reasonably correlate the microscopic aggregation modes with the macroscopic morphologies observed by SEM and TEM. These results are useful as a potential database to design new porphyrin-based gelators. So far, the hydrogen-bonding interaction and van der Waals interaction have been raised as major driving forces for gel formation. It should be emphasized, from the present study, that, in addition to these interactions, the dipole−dipole interaction also plays an important role in the gel formation process to affect the molecular assembling mode leading to the final morphology. We believe that the creation of novel porphyrin aggregation modes is possible by combining these interactions, which would lead to new functional properties arising from the porphyrin-based unique superstructures.

Experimental Section

General. All starting materials and solvents were purchased from Tokyo Kasei Organic Chemicals, Wako Organic Chemicals, or Aldrich and used as received. The ^{1}H NMR spectra were recorded either on a Bruker AC 250 (250 MHz) spectrometer or on a Bruker DRX 600 (600 MHz) spectrometer. Chemical shifts are reported in ppm downfield from tetramethylsilane as the internal standard. Mass spectral data were obtained using a Perseptive Voyager RP matrix assisted laser desorption/ionization-time of flight (MALDI-TOF) mass spectrometer and/or a JEOL JMS HX110A high-resolution magnetic sector fast atom bombardment (FAB) mass spectrometer. UV−vis spectra were recorded with a Shimadzu UV-2500 PC spectrophotometer.

Measurement of Sol−Gel Transition Temperatures. The sealed tube containing the gel was immersed inversely in a thermostated oil bath. The temperature was raised at a rate of 1 °C min^{-1}. Here, T_{gel} was defined as the temperature at which the gel was broken.

FT-IR Measurement of Xerogels and Solids. All FT-IR measurements of xerogels and solids were performed in attenuated total reflection (ATR).

Powder X-ray Diffraction. The gel was prepared in a sample tube and frozen by liquid nitrogen. The frozen specimen was evaporated by a vacuum pump at 0.6 mmHg for 1 day at room temperature. The obtained xerogel was put into a glass capillary ($\Phi = 0.3$ mm). An X-ray diffractogram was recorded on an imaging plate using Cu radiation ($\lambda = 1.541\,78$ Å at a distance of 15 cm).

SEM Observation. The gel was prepared in a sample tube and frozen by liquid nitrogen. The frozen specimen was evaporated by a vacuum pump at 0.6 mmHg for 1 day at room temperature. The obtained xerogel was shielded with platin. The accelerating voltage of the scanning electron microscope was 25 kV, and the emission current was 10 μA.

TEM Observation. A piece of the gel was placed on a carbon-coated copper grid. The specimen was evaporated by a vacuum pump at 0.6 mmHg for 1 day at room temperature. The

Scheme 1

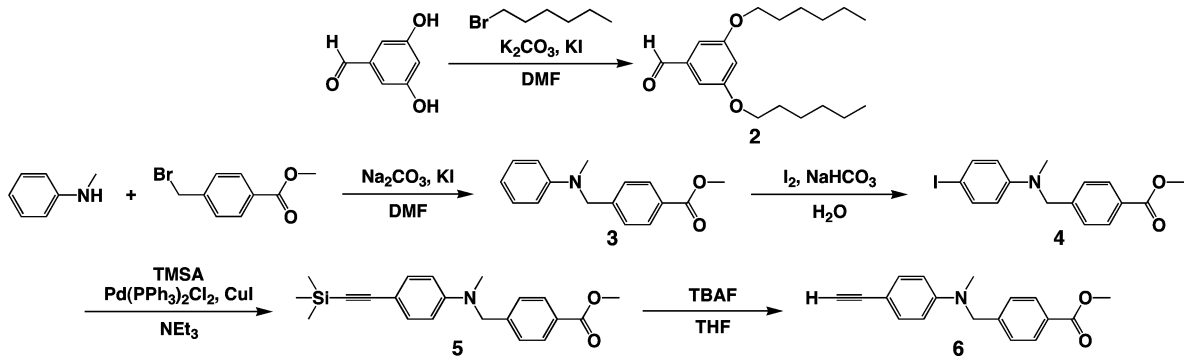

Scheme 2

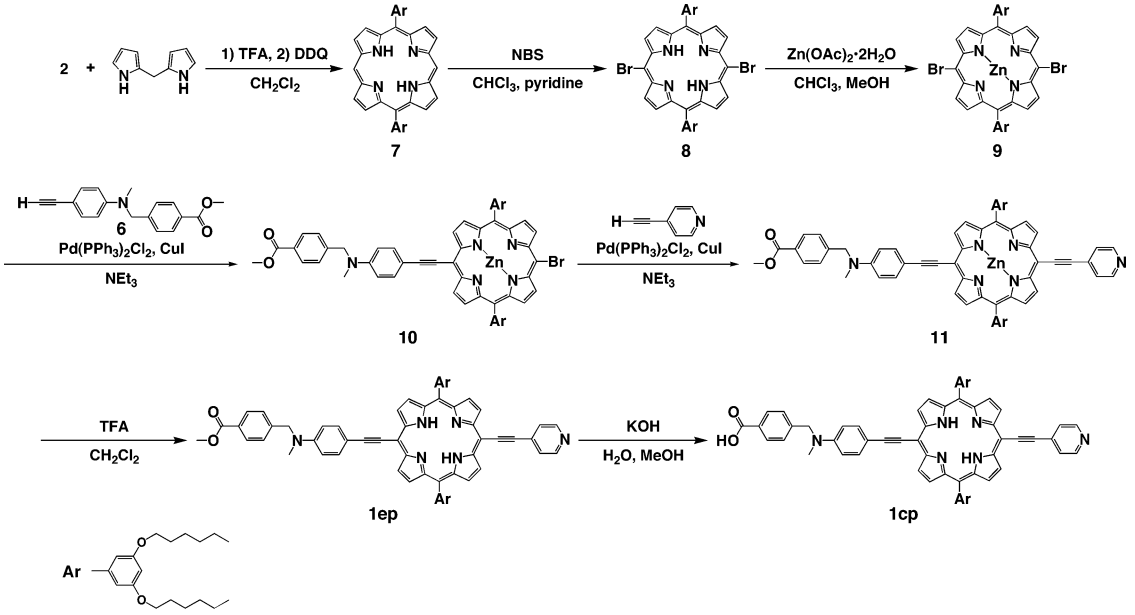

Scheme 3

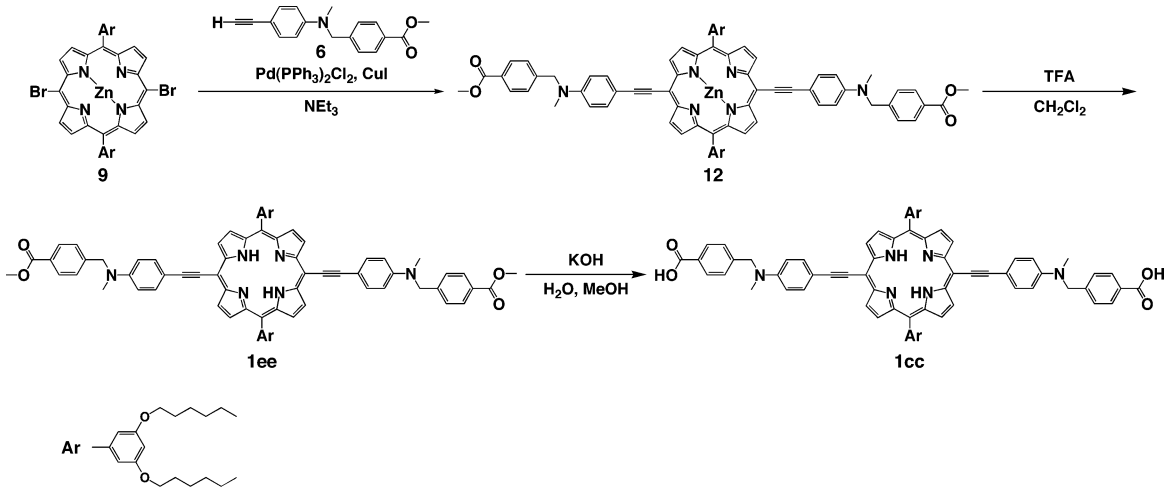

accelerating voltage of the transmission electron microscope was 120 kV, and the beam current was 65 μA.

Synthesis. Compounds **1cp**, **1ep**, **1ee**, **1pp**, and **1cc** were synthesized according to Schemes 1−4 and identified by ^{1}H NMR, high-resolution FAB mass measurements, and/or elemental analyses. Compound **2** was synthesized according to the reported procedure.[20]

Methyl 4-(*N*-Methyl-*N*-phenylaminomethyl)benzoate (3). Compound **3** was synthesized by the method reported by Gokel et al.[21] *N*-Methylaniline (2.00 mL, 18.7 mmol), methyl 4-(bromomethyl)benzoate (4.70 g, 20.5 mmol), Na_2CO_3 (7.90 g, 74.6 mmol), and KI (0.77 g, 4.67 mmol) were dissolved in dimethylformamide (DMF) (100 mL). The solution was stirred for 24 h at 65 °C under N_2. The reaction progress was monitored by thin-layer chromatography (TLC) [silica gel, $CHCl_3$/*n*-hexane = 3:1 (v/v)]. After cooling the mixture to room temperature, DMF was removed under vacuum. $CHCl_3$ was added to the resulting

(20) Meier, H.; Dullweber, U. *J. Org. Chem*. **1997**, *62*, 4821−4826.

(21) Schultz, R. A.; White, D. B.; Dishong, D. M.; Arnold, K. A.; Gokel, G. W. *J. Am. Chem. Soc.* **1985**, *107*, 6659−6668.

Scheme 4

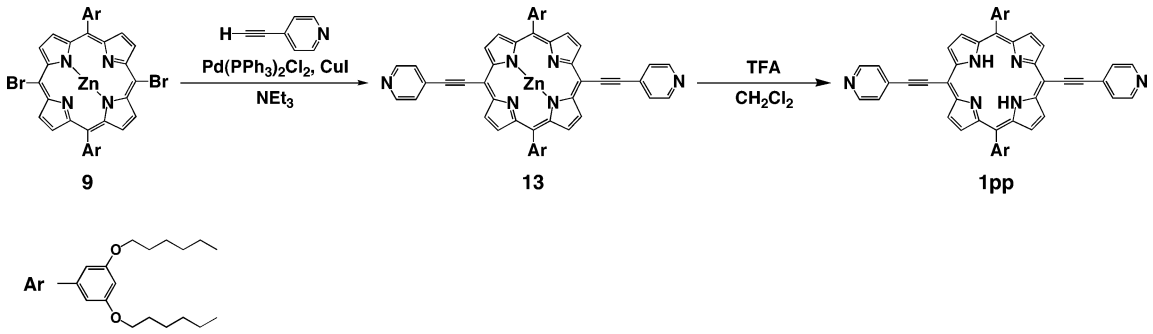

residue, and the solution was washed with water. The organic layer was dried over anhydrous $MgSO_4$ and concentrated under reduced pressure. The resulting residue was subjected to column chromatography (silica gel, CH_2Cl_2) to give **3** in 52% yield (2.50 g) as yellow oil. ^{1}H NMR (250 MHz, $CDCl_3$, TMS, rt): δ 3.03 (s, 3H), 3.89 (s, 3H), 4.57 (s, 2H), 6.73 (m, 3H), 7.22 (t, J = 7.2, 2H), 7.29 (d, J = 7.9, 2H), 7.98 (d, J = 8.0, 2H). MALDI-TOF-MS [dithranol] *m/z* calcd for $[M + H]^+$, 256.13; found, 256.16. Anal. Calcd for $C_{16}H_{17}NO_2 \cdot 0.50H_2O$: C, 72.70; H, 6.86; N, 5.30. Found: C, 72.91; H, 6.52; N, 5.28.

Methyl 4-[*N*-Methyl-*N*-(4′-iodophenyl)aminomethyl]benzoate (4). A solution of **3** (2.00 g, 7.83 mmol) and $NaHCO_3$ (1.00 g, 11.8 mmol) in H_2O was stirred in an ice bath. After the addition of I_2 (1.80 g, 7.12 mmol), the solution was stirred for 1 h at room temperature. The solution was diluted by ether, and the organic solution was washed with aqueous $Na_2S_2O_3$ and water. The organic layer was separated and dried over anhydrous $MgSO_4$ and concentrated under reduced pressure. The resulting residue was subjected to column chromatography [silica gel, CH_2Cl_2/*n*-hexane = 3:1 (v/v)] to give **4** in 77% yield (2.3 g) as white solid. mp 87.9−89.2 °C. ^{1}H NMR (250 MHz, $CDCl_3$, TMS, rt): δ 3.02 (s, 3H), 3.90 (s, 3H), 4.55 (s, 2H), 6.47 (d, J = 8.1, 3H), 7.25 (d, J = 6.2, 2H), 7.44 (d, J = 8.0, 2H), 7.98 (d, J = 7.5, 2H). MALDI-TOF-MS [dithranol] *m/z* calcd for $[M + H]^+$, 382.02; found, 382.09. Anal. Calcd for $C_{16}H_{16}INO_2$: C, 50.41; H, 4.23; N, 3.67. Found: C, 50.62; H, 4.36; N, 3.59.

Methyl 4-[*N*-Methyl-*N*-(4′-trimethylsilylethynylphenyl)-aminomethyl]benzoate (5). Compound **4** (2.00 g, 5.25 mmol), trimethylsilylacetylene (1.55 g, 15.8 mmol), $Pd(PPh_3)_2Cl_2$ (0.37 g, 0.53 mmol), and CuI (0.15 g, 0.80 mmol) were mixed in dry triethylamine (30 mL). The mixture was stirred for 2 h at room temperature under N_2. The reaction progress was monitored by TLC [silica gel, CH_2Cl_2/*n*-hexane = 1:1 (v/v)]. The solution was concentrated under reduced pressure, and the resulting residue was washed with saturated ammonium chloride and water. The organic layer was dried over anhydrous $MgSO_4$ and concentrated under reduced pressure. The resulting residue was subjected to column chromatography [silica gel, CH_2Cl_2/*n*-hexane = 1:1 (v/v)] to give **5** in >99% yield (2.1 g) as brown oil. ^{1}H NMR (250 MHz, $CDCl_3$, TMS, rt): δ 0.22 (s, 9H), 3.05 (s, 3H), 3.90 (s, 3H), 4.59 (s, 2H), 6.59 (d, J = 8.7, 3H), 7.24 (d, J = 8.6, 2H), 7.31 (d, J = 8.7, 2H), 7.97 (d, J = 8.2, 2H). MALDI-TOF-MS [dithranol] *m/z* calcd for $[M + H]^+$, 352.17; found, 352.24. Anal. Calcd for $C_{21}H_{25}NO_2Si \cdot 0.25CH_2Cl_2$: C, 68.47; H, 6.90; N, 3.76. Found: C, 68.41; H, 6.83; N, 3.74.

Methyl 4-[*N*-Methyl-*N*-(4′-ethynylphenyl)aminomethyl]-benzoate (6). Compound **5** (1.80 g, 5.12 mmol) was dissolved in tetrahydrofuran (THF) (35 mL). Tetrabutylammonium fluoride (TBAF) (10.2 mL, 1 M in THF) was added, and the mixture was stirred for 1 h at room temperature. The reaction progress was monitored by TLC (silica gel, $CHCl_3$). The solution was concentrated under reduced pressure, and the resulting residue was subjected to column chromatography (silica gel, $CHCl_3$) to give **6** in 71% yield (1.0 g) as brown solid. mp 91.7−93.5 °C. ^{1}H NMR (250 MHz, $CDCl_3$, TMS, rt): δ 2.97 (s, 1H), 3.07 (s, 3H), 3.90 (s, 3H), 4.60 (s, 2H), 6.62 (d, J = 8.5, 3H), 7.26 (d, J = 7.9, 2H), 7.34 (d, J = 8.4, 2H), 7.99 (d, J = 8.0, 2H). MALDI-TOF-MS [dithranol] *m/z* calcd for $[M + H]^+$, 280.13; found, 280.18. Anal. Calcd for $C_{18}H_{17}INO_2 \cdot 0.25THF$: C, 76.74; H, 6.44; N, 4.71. Found: C, 76.85; H, 6.15; N, 5.02.

5,15-Bis(3′,5′-di-*n*-hexyloxyphenyl)porphyrin (7). Compound **7** was synthesized from 2,2′-dipyrromethane and **2** by the method reported by Manka and Lawrence.[22] 2,2′-Dipyrromethane (0.82 g, 5.52 mmol) and **2** (1.69 g, 5.52 mmol) were dissolved in CH_2Cl_2 (1.1 L). After the addition of trifluoroacetic acid (TFA) (0.30 mL), the solution was stirred for 4 h at room temperature under N_2 in the dark. Then, 2,3-dichloro-5,6-dicyano-1,4-benzoquinone (DDQ) (1.63 g, 7.18 mmol) was added to the solution, and the reaction mixture was stirred for 30 min. The reaction mixture was passed through a silica pad ($CHCl_3$) directly. Further purification by column chromatography (silica gel, $CHCl_3$) gave **7** in 36% yield (900 mg) as purple solid. mp 116.9−117.9 °C. ^{1}H NMR (600 MHz, $CDCl_3$, TMS, rt): δ −3.15 (s, 2H), 0.90 (t, J = 6.9, 12H), 1.31−1.39 (m, 16H), 1.52 (m, 8H), 1.88 (m, 8H), 4.16 (t, J = 6.7, 8H), 6.92 (s, 2H), 7.42 (d, J = 2.2, 4H), 9.19 (d, J = 4.5, 4H), 9.38 (d, J = 4.5, 4H), 10.29 (s, 2H). MALDI-TOF-MS [dithranol] *m/z* calcd, 864.18; found, 864.58. Anal. Calcd for $C_{56}H_{70}N_4O_4$: C, 77.92; H, 8.17; N, 6.49. Found: C, 77.68; H, 8.13; N, 6.49.

5,15-Dibromo-10,20-bis(3′,5′-di-*n*-hexyloxyphenyl)porphyrin (8). Compound **8** was synthesized from **7** by the method reported by Therien et al.[23] Compound **7** (880 mg, 1.02 mmol) was dissolved in $CHCl_3$ (250 mL) and cooled to 0 °C. *N*-bromosuccinimide (NBS) (363 mg, 2.04 mmol) and pyridine (1.0 mL) were added to the solution, and the mixture was stirred for 15 min at 0 °C. The reaction progress was monitored by TLC [silica gel, $CHCl_3$/*n*-hexane = 1:1 (v/v)]. The reaction was quenched with acetone (4.0 mL), and the solution was concentrated under reduced pressure. The resulting residue was subjected to column chromatography [silica gel, $CHCl_3$/*n*-hexane = 1:1 (v/v)] to give **8** in 88% yield (920 mg) as sticky purple solid. ^{1}H NMR (600 MHz, $CDCl_3$, TMS, rt): δ −2.75 (s, 2H), 0.90 (t, J = 6.9, 12H), 1.33−1.40 (m, 16H), 1.51 (m, 8H), 1.88 (m, 8H), 4.13 (t, J = 6.6, 8H), 6.90 (s, 2H), 7.31 (d, J = 2.1, 4H), 8.96 (s (br), 4H), 9.60 (d, J = 4.5, 4H). MALDI-TOF-MS [dithranol] *m/z* calcd, 1021.97; found, 1021.62. Compound **8** was used for the synthesis of **9** without further purification.

5,15-Dibromo-10,20-bis(3′,5′-di-*n*-hexyloxyphenyl)porphyrinatozinc (9). Compound **8** (700 mg, 0.68 mmol) was dissolved in $CHCl_3$ (200 mL). After the addition of a methanol solution (40 mL) of $Zn(OAc)_2 \cdot 2H_2O$ (1.49 g, 6.80 mmol), the solution was stirred for 1 h at room temperature. The solution was concentrated under reduced pressure, and the resulting residue was washed with water. The organic layer was dried over anhydrous Na_2SO_4 and concentrated under reduced pressure to give **9** in 95% yield (700 mg) as purple solid. mp 220.0−224.7 °C. ^{1}H NMR (250 MHz, $CDCl_3$, TMS, rt): δ 0.90 (m, 12H), 1.32−1.38 (m, 16H), 1.49 (m, 8H), 1.86 (m, 8H), 4.10 (t, J = 6.6, 8H), 6.86 (s, 2H), 7.29 (s, 4H), 9.05 (d, J = 4.7, 4H), 9.69 (d, J = 4.7, 4H). MALDI-TOF-MS [dithranol] *m/z* calcd, 1085.35; found, 1085.35. Anal. Calcd for $C_{56}H_{66}Br_2N_4O_4Zn$: C, 62.03; H, 6.13; N, 5.17. Found: C, 61.85; H, 6.16; N, 5.07.

Compound 10. Compound **9** (496 mg, 0.46 mmol), **6** (153 mg, 0.55 mmol), $Pd(PPh_3)_2Cl_2$ (17.5 mg, 25.0 μmol), and CuI (7.2 mg, 38 μmol) were mixed in dry triethylamine (35 mL). The mixture

(22) Manka, J. S.; Lawrence D. L. *Tetrahedron Lett.* **1989**, *30*, 6989−6902.

(23) (a) DiMagno, S. G.; Lin, V. S.-Y.; Therien, M. J. *J. Am. Chem. Soc.* **1993**, *115*, 2513−2515. (b) DiMagno, S. G.; Lin, V. S.-Y.; Therien, M. J. *J. Org. Chem.* **1993**, *58*, 5983−5993.

was stirred for 3 h at room temperature under N_2. The reaction progress was monitored by TLC [silica gel, CH_2Cl_2/*n*-hexane = 3:1 (v/v)]. The solution was concentrated under reduced pressure, and the resulting residue was washed with saturated ammonium chloride aqueous solution and water. The organic layer was dried over anhydrous Na_2SO_4 and concentrated under reduced pressure. The resulting residue was subjected to column chromatography [silica gel, CH_2Cl_2/*n*-hexane = 3:1 (v/v)] to give **10** in 40% yield (235 mg) as green solid. mp 224.6−226.7 °C. ^{1}H NMR (600 MHz, $CDCl_3$, TMS): δ 0.90 (t, J = 6.9, 12H), 1.32 (m, 16H), 1.51 (m, 8H), 1.88 (m, 8H), 3.06 (s, 3H), 3.89 (s, 3H), 4.13 (t, J = 6.6, 8H), 4.55 (s, 2H), 6.61 (d, J = 8.4, 2H), 6.89 (s, 2H), 7.28 (d, J = 8.2, 2H), 7.34 (d, J = 1.6, 4H), 7.61 (d, J = 8.4, 2H), 7.99 (d, J = 8.3, 2H), 9.03 (m, 4H), 9.66 (d, J = 4.6, 2H), 9.70 (d, J = 4.5, 2H). MALDI-TOF-MS [dithranol] *m/z* calcd, 1283.77; found, 1283.44. Anal. Calcd for $C_{74}H_{82}BrN_5O_6Zn$: C, 69.29; H, 6.44; N, 5.46. Found: C, 69.09; H, 6.48; N, 5.46.

Compound 11. Compound **10** (200 mg, 0.16 mmol), 4-ethynylpyridine (80.4 mg, 0.78 mmol), $Pd(PPh_3)_2Cl_2$ (10.9 mg, 15.6 μmol), and CuI (4.5 mg, 23 μmol) were mixed in dry triethylamine (12 mL). The mixture was stirred for 24 h at room temperature under N_2. The reaction progress was monitored by TLC (silica gel, $CHCl_3$). The solution was concentrated under reduced pressure, and the resulting residue was washed with saturated ammonium chloride aqueous solution and water. The organic layer was dried over anhydrous Na_2SO_4 and concentrated under reduced pressure. The resulting residue was subjected to column chromatography (silica gel, $CHCl_3$) to give **11** in 77% yield (157 mg) as green solid. mp 244.5−246.6 °C. ^{1}H NMR (600 MHz, pyridine-d_5, TMS, rt): δ 0.84 (t, J = 6.9, 12H), 1.26 (m, 16H), 1.49 (m, 8H), 1.87 (m, 8H), 3.07 (s, 3H), 3.84 (s, 3H), 4.19 (t, J = 6.5, 8H), 4.70 (s, 2H), 7.03 (d, J = 8.7, 2H), 7.32 (s, 2H), 7.41 (t, J = 8.2, 2H), 7.75 (d, J = 2.0, 4H), 7.97 (d, J = 5.6, 2H), 8.17 (d, J = 8.8, 2H), 8.19 (d, J = 8.3, 2H), 8.95 (d, J = 5.7, 2H), 9.35 (d, J = 4.4, 2H), 9.41 (d, J = 4.5, 2H), 10.08 (d, J = 4.5, 2H), 10.17 (d, J = 4.5, 2H). HR-FAB [NBA] *m/z* calcd for $[M]^+$, 1302.5900; found, 1302.5902.

Compound 1ep. Compound **11** (190 mg, 0.15 mmol) was dissolved in CH_2Cl_2 (50 mL). After the addition of TFA (0.50 mL), the solution was stirred for 30 min at room temperature. The reaction mixture was washed with 5% aqueous ammonia solution and water. The organic layer was dried over anhydrous Na_2SO_4. The solution was concentrated under reduced pressure. The resulting residue was subjected to column chromatography (silica gel, $CHCl_3$) to give **1ep** in 93% yield (133 mg) as green solid. mp 224.1−226.1 °C. ^{1}H NMR (600 MHz, $CDCl_3$, TMS, rt): δ −2.34 (s, 2H), 0.90 (t, J = 6.8, 12H), 1.36 (m, 16H), 1.52 (m, 8H), 1.88 (m, 8H), 3.21 (s, 3H), 3.93 (s, 3H), 4.14 (t, J = 6.6, 8H), 4.74 (s, 2H), 6.88 (d, J = 8.5, 2H), 6.91 (s, 2H), 7.34 (m, 6H), 7.85 (d, J = 5.2, 2H), 7.87 (d, J = 8.4, 2H), 8.05 (d, J = 8.1, 2H), 8.81 (d, J = 4.9, 2H), 8.91 (d, J = 4.1, 2H), 8.96 (d, J = 4.3, 2H), 9.58 (d, J = 4.5, 2H), 9.64 (d, J = 4.5, 2H). HR-FAB [NBA] *m/z* calcd for $[M]^+$, 1240.6765; found, 1240.6807.

Compound 1cp. Compound **1ep** (50 mg, 40 μmol) was dissolved in THF (10 mL). KOH [1 mL of 2 M solution in H_2O/MeOH = 1:4 (v/v)] was added, and the mixture was refluxed for 3 h. The reaction progress was monitored by TLC [silica gel, $CHCl_3$/MeOH = 25:1 (v/v)]. After cooling the mixture to room temperature, the solution was concentrated under reduced pressure. The resulting residue was washed with water. The organic layer was dried over anhydrous Na_2SO_4 and concentrated under reduced pressure. The resulting residue was subjected to column chromatography (silica gel, $CHCl_3$) to give **1cp** in 81% yield (40 mg) as green solid. mp 238.9−242.9 °C; ^{1}H NMR (600 MHz, CD_2Cl_2/pyridine-d_5, TMS, rt): δ −1.69 (s, 2H), 0.83 (t, J = 6.7, 12H), 1.32 (m, 16H), 1.51 (m, 8H), 1.87 (m, 8H), 3.12 (s, 3H), 4.15 (t, J = 6.5, 8H), 4.69 (s, 2H), 6.93 (d, J = 8.5, 2H), 7.07 (s, 2H), 7.37 (d, J = 8.0, 2H), 7.46 (s, 2H), 7.86 (d, J = 4.8, 2H), 7.98 (d, J = 8.4, 2H), 8.26 (d, J = 8.0, 2H), 8.82 (d, J = 4.8, 2H), 9.03 (d, J = 4.3, 2H), 9.08 (d, J = 4.3, 2H), 9.74 (d, J = 4.5, 2H), 9.81 (d, J = 4.5, 2H). MALDI-TOF-MS [dithranol] *m/z* calcd, 1228.58; found, 1228.90. Anal. Calcd for $C_{80}H_{86}N_6O_6$: C, 78.27; H, 7.06; N, 6.85. Found: C, 78.00; H, 7.13; N, 6.80.

Compound 12. Compound **9** (100 mg, 92.2 μmol), **6** (128 mg, 0.46 mmol), $Pd(PPh_3)_2Cl_2$ (6.5 mg, 9.2 μmol), and CuI (2.6 mg, 14 μmol) were mixed in dry triethylamine (5 mL). The mixture was stirred for 4 h at room temperature under N_2. The reaction progress was monitored by TLC (silica gel, CH_2Cl_2). The solution was concentrated under reduced pressure, and the resulting residue was washed with saturated ammonium chloride aqueous solution and water. The organic layer was dried over anhydrous Na_2SO_4 and concentrated under reduced pressure. The resulting residue was subjected to column chromatography (silica gel, CH_2Cl_2) to give **12** in 86% yield (137 mg) as green solid. mp >245 °C (decomp). ^{1}H NMR (600 MHz, $CDCl_3$, TMS, rt): δ 0.90 (t, J = 6.9, 12H), 1.38 (m, 16H), 1.52 (m, 8H), 1.88 (m, 8H), 3.07 (s, 6H), 3.90 (s, 6H), 4.15 (t, J = 6.6, 8H), 4.56 (s, 4H), 6.64 (d, J = 8.5, 4H), 6.90 (s, 2H), 7.29 (d, J = 8.2, 4H), 7.37 (d, J = 2.0, 4H), 7.65 (d, J = 8.5, 4H), 8.01 (d, J = 8.3, 4H), 9.00 (d, J = 4.5, 4H), 9.67 (d, J = 4.5, 4H). MALDI-TOF-MS [dithranol] *m/z* calcd, 1482.19; found, 1482.86. Anal. Calcd for $C_{92}H_{98}N_6O_8Zn$: C, 74.60; H, 6.67; N, 5.67. Found: C, 74.68; H, 6.87; N, 5.39.

Compound 1ee. Compound **12** (200 mg, 0.14 mmol) was dissolved in CH_2Cl_2 (60 mL). After the addition of TFA (0.60 mL), the solution was stirred for 30 min at room temperature. The reaction mixture was washed with 5% aqueous ammonia solution and water. The organic layer was dried over anhydrous Na_2SO_4. The solution was concentrated under reduced pressure. The resulting residue was subjected to column chromatography (silica gel, $CHCl_3$) to give **1ee** in 65% yield (124 mg) as green solid. mp 215.2−216.2 °C. ^{1}H NMR (600 MHz, $CDCl_3$, TMS, rt): δ −1.81 (s, 2H), 0.90 (t, J = 6.6, 12H), 1.36 (m, 16H), 1.51 (m, 8H), 1.88 (m, 8H), 3.20 (s, 6H), 3.92 (s, 6H), 4.13 (t, J = 6.5, 4H), 4.72 (s, 4H), 6.87 (m, 2H + 4H), 7.34 (m, 4H + 4H), 7.86 (d, J = 8.3, 4H), 8.04 (d, J = 8.1, 4H), 8.88 (d, J = 3.9, 4H), 9.60 (d, J = 4.4, 4H). HR-FAB [NBA] *m/z* calcd for $[M]^+$, 1416.7603; found, 1416.7607.

Compound 1cc. Compound **1ee** (120 mg, 84.6 μmol) was dissolved in THF (20 mL). KOH [2 mL of 2 M solution in H_2O/MeOH = 1:4 (v/v)] was added, and the mixture was refluxed for 3 h. The reaction progress was monitored by TLC [silica gel, $CHCl_3$/MeOH = 25:1 (v/v)]. After cooling the mixture to room temperature, the solution was concentrated under reduced pressure. The resulting residue was washed with 1 M aqueous HCl solution and water. The organic layer was dried over anhydrous Na_2SO_4 and concentrated under reduced pressure. The resulting residue was subjected to column chromatography [silica gel, $CHCl_3$ /MeOH = 10:1 (v/v)] to give **1cc** in 49% yield (58 mg) as green solid. mp >290 °C (decomp). ^{1}H NMR (600 MHz, CD_2Cl_2/pyridine-d_5, TMS, rt): δ −1.52 (s, 2H), 0.87 (t, J = 7.0, 12H), 1.30 (m, 16H), 1.49 (m, 8H), 1.86 (m, 8H), 3.10 (s, 6H), 4.14 (t, J = 6.5, 8H), 4.68 (s, 4H), 6.93 (d, J = 8.7, 4H), 7.07 (s, 2H), 7.37 (d, J = 8.1, 4H), 7.46 (d, J = 1.8, 4H), 7.97 (d, J = 8.7, 4H), 8.27 (d, J = 8.2, 4H), 9.02 (d, J = 4.5, 4H), 9.79 (d, J = 4.6, 4H). HR-FAB [NBA] *m/z* calcd for $[M]^+$, 1388.7290; found, 1388.7296.

Compound 1pp. Compound **9** (100 mg, 92.2 μmol), 4-ethynylpyridine (47.5 mg, 0.46 mmol), $Pd(PPh_3)_2Cl_2$ (6.5 mg, 9.2 μmol), and CuI (2.6 mg, 14 μmol) were mixed in dry triethylamine (5 mL). The mixture was stirred for 4 h at room temperature under N_2. The reaction progress was monitored by TLC [silica gel, $CHCl_3$/MeOH = 25:1 (v/v)]. The solution was concentrated under reduced pressure, and the resulting residue was washed with saturated ammonium chloride aqueous solution and water. The organic layer was dried over anhydrous Na_2SO_4 and concentrated under reduced pressure. The resulting residue was subjected to column chromatography [silica gel, $CHCl_3$/MeOH = 25:1 (v/v)] to give **13** in 79% yield (82 mg) as green solid. MALDI-TOF-MS [dithranol] *m/z* calcd, 1129.76; found, 1129.60. Compound **13** was used for the synthesis of **1pp** without further purification.

Compound **13** (82 mg, 73 μmol) was dissolved in CH_2Cl_2 (35 mL). After the addition of TFA (0.30 mL), the solution was stirred for 30 min at room temperature. The reaction mixture was washed with 5% aqueous ammonia solution and water. The organic layer was dried over anhydrous Na_2SO_4. The solution was concentrated under reduced pressure. The resulting residue was subjected to column chromatography [silica gel, $CHCl_3$/MeOH = 25:1 (v/v)] to give **1pp** in 91% yield (70 mg) as green solid. mp >300 °C (decomp). ^{1}H NMR (600 MHz, CD_2Cl_2, TMS, rt): δ −2.15 (s, 2H), 0.91 (t, J = 6.8, 12H), 1.38 (m, 16H), 1.52 (m, 8H), 1.88 (m, 8H), 4.16 (t, J = 6.7, 4H), 6.92 (s, 2H), 7.35 (d, J = 1.9, 4H), 7.87 (d,

$J = 3.4$, 4H), 8.73 (br, 4H), 9.02 (d, $J = 3.9$, 4H), 9.67 (d, $J = 4.4$, 4H). HR-FAB [NBA] *m/z* calcd for $[M]^+$, 1064.5928; found, 1064.5929.

Acknowledgment. We thank Ms. S. Kanae and Ms. E. Okasaki at Kyushu University for ^{1}H NMR and HRMS measurements. The present work is partially supported by a Grant-in-Aid for the 21st Century COE Program "Functional Innovation of Molecular Informatics" from the Ministry of Education, Culture, Science, Sports and Technology of Japan.

Supporting Information Available: ^{1}H NMR spectra of **1ep**, **1cp**, **1ee**, **1cc**, and **1pp**. This material is available free of charge via the Internet at http://pubs.acs.org.

LA047070U